Journal of Catalysis 413 (2022) 1111–1122

Contents lists available at ScienceDirect

Journal of Catalysis

journal homepage: www.elsevier.com/locate/jcat

Identification and quantification of multinuclear Cu active sites derived from monomeric Cu moieties for dry NO oxidation over Cu-SSZ-13

Ishant Khurana *, Jonatan D. Albarracin-Caballero, Arthur J. Shih *,[1]

Davidson School of Chemical Engineering, Purdue University, West Lafayette, IN 47907, USA

ARTICLE INFO

Article history:
Received 12 May 2022
Revised 5 August 2022
Accepted 6 August 2022
Available online 17 August 2022

Keywords:
Kinetics
Turnover
Solvation
Active site
Mechanism
NO oxidation
SSZ-13
CO-TPR
Cu-oxo
Dimers

ABSTRACT

The identification and quantification of multinuclear Cu-oxo cations in Cu-zeolites is a challenge amidst the dynamic nature of Cu ions in Cu-zeolites. Herein, we synthesized Cu-SSZ-13 zeolites containing varying densities of monomeric Cu cations (Z_2Cu and ZCuOH, where Z represents an anionic site on the zeolite framework). The number of Cu-oxo cations, quantified using carbon monoxide temperature programmed reduction (CO-TPR), quadratically increased with increasing ZCuOH density, evidencing that proximal ZCuOH sites are precursors to Cu-oxo dimers. We also find that dehydrated proximal ZCuOH with overlapping diffusion radii of at most 0.5 nm can form Cu-oxo dimers. CO-TPR also revealed the presence of three distinct pools (i.e types) of Cu-oxo dimers; these pools catalyze dry NO oxidation at different turnover rates, with the fastest pool 2 to 30 times faster than the slowest pool. From reaction kinetics and rate law analysis, we also proposed a cohesive dry NO oxidation mechanism and demonstrated that nitrates detected by in situ FTIR are a spectator species.

1. Introduction

1.1. Current understanding of Cu species in Cu-SSZ-13 zeolites

Copper-exchanged SSZ-13 zeolites are a class of catalysts that has found commercial success for the selective catalytic reduction of NO_x with NH_3 (SCR) because of its higher hydrothermal stability compared to other zeolites [1–4]. Monomeric Cu^{2+} cations present near the six-membered ring of SSZ-13 were first proposed as the active site for standard SCR [5–8]. Further studies demonstrated that Cu^{2+} are found at two different cationic positions, indicating two different types of Cu^{2+} cations [9–12]. It is now known that monomeric Cu exist as two distinct types: the first type a Cu^{2+} charge-balanced by two anionic sites in the double six membered ring (D6R) of the CHA structure (hereafter denoted as Z_2Cu, where Z indicates an anionic site on the zeolite) and the second type a $[CuOH]^{1+}$ charge-balanced by one framework Al atom (hereafter denoted as ZCuOH). The relative fractions of Z_2Cu and ZCuOH depend on zeolite framework's Al density and distribution [13,14]. Both Z_2Cu and ZCuOH catalyze standard SCR at similar turnover rates [13,15–17]. More importantly, transformations of Z_2Cu and ZCuOH sites have been tracked as they evolve under different gas exposure conditions, from ambient conditions (monomeric, solvated by H_2O, mobile), to dry and inert high temperature treatment (dehydrated, electronically tethered to the zeolite), to NH_3-SCR *operando* conditions (solvated by NH_3, more mobile) [18].

Efforts have been directed towards identifying Cu_3O_y [19] and Cu_2O_y [19–21] species formed at high temperature oxidative treatment (~673 K in 20 % O_2) in Cu-SSZ-13 and Cu-MOR. Ipek et al. [21] utilized UV–visible and Raman spectroscopy to detect and propose various reactive Cu_2O_y species such as $[Cu–O_2–Cu]^{2+}$ (*trans*-μ-1,2-peroxo dicopper(II)), and $[Cu–O–Cu]^{2+}$ (mono-(μ–oxo) dicopper (II)). Such species have been proposed to evolve from $[CuOH]^+$ precursors under high temperature oxidative treatment (10 % O_2 at 773 K), either from direct reaction of auto-reduced Cu^{1+} with O_2, forming $[Cu–O_2–Cu]^{2+}$, or from the condensation of proximal $[CuOH]^+$ species, resulting e.g. in mono-(μ-oxo) dicopper cores, giving $[Cu–O–Cu]^{2+}$ [20,21]. We note that these dimeric Cu_2O_y species arising from nominally monomeric $[CuOH]^+$ species are different than dimeric $[(NH_3)_2Cu-O_2-Cu(NH_3)_2]^{2+}$ species (from reaction of dioxygen with mobile Cu diamine [22–25]) and Cu_xO_y species

* Corresponding authors.
E-mail addresses: ikhuran@purdue.edu (I. Khurana), ajyshih@umich.edu, arthur.shih@northwestern.edu (A.J. Shih).
[1] Current address: Department of Materials Science and Engineering, Northwestern University, Evanston, IL 60208, USA.

https://doi.org/10.1016/j.jcat.2022.08.005
0021-9517/

(clustered Cu^{2+} ions with $x \geq 2$, $y \geq 1$ which result from over-exchange of Cu [7,26,27]). Verma et al. [26] demonstrated that clustered Cu_xO_y species can catalyze dry NO oxidation by while monomeric Z_2Cu are inert. Gao et al. [12,28] synthesized Cu-SSZ-13 with higher Cu loadings (Si:Al = 6, Cu:Al > 0.3), where ZCuOH species are expected, and detected activity for dry NO oxidation. Though the community had not indisputably confirmed the presence of ZCuOH species at time of publication, Gao et al. [12,28] hypothesized that Cu dimers were the likely species responsible for dry NO oxidation.

1.2. Disparities between dry NO oxidation and SCR

Early on, NO oxidation to gas phase NO_2 was proposed to be a key elementary step during the standard SCR reaction [1,28–30]. However, gas phase NO_2 may not be directly involved in the standard SCR reaction for a number of reasons, many of which were originally reported in Ruggeri et al. [31]. First, the dry NO to NO_2 oxidation rate is orders of magnitude lower than the standard SCR reaction rate [7,26,32]. Second, while NO_2 has a promotional effect on the standard NH_3-SCR reaction rate, NO_2 has been shown to inhibit dry NO oxidation [26,31,33]. Third, dry NO oxidation is inhibited by H_2O, which, on the contrary, has negligible [22,26,31,33–35], positive [36–38], and negative [37,38] impacts on standard NH_3-SCR. Fourth, Cu ions during NH_3-SCR are solvated by NH_3 ligands and are thus mobile whereas under dry NO oxidation conditions, the absence of NH_3 and H_2O indicates that Cu ions are less mobile [13,22]. Fifth, Z_2Cu species, which have shown to be active for NH_3-SCR, are not active for dry NO oxidation [7,26].

Several have attempted to reconcile these disparities by postulating that reaction rates measured during NO oxidation cannot be representative of the NO to NO_2 oxidation rate under SCR reaction conditions [39–42]. For instance, Khivantsev et al. [42] argued that under standard SCR reaction conditions, NH_3 could react with surface nitrosyl, nitrate, and nitrite groups and thus accelerate the desorption or consumption of NO_2. However, with this large number of disparities, we propose that the chemistries that occur during NH_3-SCR and dry NO oxidation are not directly related, and each separately provide intriguing case studies.

In this work, we synthesized a series of Cu-SSZ-13 catalysts of varying Cu cation density with only monomeric Cu cations (Z_2Cu and ZCuOH) and no clustered Cu_xO_y extraframework species. We identified two pools of Cu inactive for dry NO oxidation (dead pools) and three pools of Cu-oxo dimers active for dry NO oxidation (active pools). Across the three active pools, turnover rates were shown to differ by 2 to 30 times. Kinetic evidence was then used to propose a cohesive catalytic dry NO oxidation mechanism. An understanding of Cu-oxo speciation has implications for reactions beyond dry NO oxidation, such as methane upgrading [43–55], benzene to phenols [56], NO decomposition [57–61], and oxidation of volatile organic compounds [62].

2. Experimental methods

2.1. Synthesis and preparation of Cu-SSZ-13

Synthesis of SSZ-13 and subsequent Cu-exchange were performed in-house. Extended details on Cu-SSZ-13 synthesis and preparation can be found in the Supplementary Information, Section S1. In brief, high-aluminum SSZ-13 zeolites (Si:Al = 4.5) were synthesized as reported by Fickel et al. [63], which is based on a patent by Zones [64]. Low aluminum SSZ-13 zeolites (Si:Al 15 to 25) were synthesized using a procedure by Deka et al. [65]. After washing and drying, the zeolite was calcined under dry air (AirZero, < 1 ppm total hydrocarbons, Indiana Oxygen Co.) at 873 K to produce Na-SSZ-13. Aqueous ion-exchange between Na^+ and NH_4^+ was performed, dried at 373 K under ambient air, then calcined under dry air (AirZero, < 1 ppm total hydrocarbons, Indiana Oxygen Co.) at 823 K. This calcination desorbed the NH_3 and resulted in H-SSZ-13.

Cu-zeolites were prepared by aqueous-phase Cu ion exchange of H-form zeolites with a $Cu(NO_3)_2$ solution (0.001 M to 0.1 M, with higher concentrations resulting in higher Cu loadings, 100 $cm^3_{solution}\ g^{-1}_{catalyst}$; 99.999 wt% $Cu(NO_3)_2$ from Sigma Aldrich) during which the pH was controlled to 4.9 ± 0.1 through dropwise addition of a 1.0 M NH_4OH solution (Sigma Aldrich, 28.0 % ammonium hydroxide solution, ACS reagent grade). Care was taken to ensure that solid hydroxide precipitates do not form during the Cu ion exchange process as they lead to undesired clustered Cu_xO_y [27]. Cu-SSZ-13 catalysts were dried at 373 K in ambient air, then calcined in dry air (100 mL $g^{-1}_{catalyst}$, AirZero, < 1 ppm total hydrocarbons, Indiana Oxygen Co.) at 773 K.

2.2. Atomic absorption spectroscopy (AAS) to determine elemental composition

~0.03 g of dry sample (H-SSZ-13 or Cu-SSZ-13) were dissolved in ~ 2 mL of hydrofluoric acid (HF) (Mallinckrodt Baker, 48 % HF, Baker Analyzed® A.C.S. Reagent) in a 60 mL high density polyethylene (HDPE) bottle (2 oz., 60 mL Nalgene™ Wide-Mouth Amber HDPE bottle). A polyethylene pipet was used to transfer the HF. The sample was capped and left to dissolve for ~ 12 h then diluted with ~ 50 mL of deionized water (Millipore, 18.2 cm·MΩ resistivity at 298 K). Bulk elemental composition was determined using atomic absorption spectroscopy (AAS) on a Perkin Elmer AAnalyst 300. Results are presented in Table S1.

2.3. Cu site characterization and quantification

Monomeric Z_2Cu and ZCuOH sites on each Cu-SSZ-13 zeolite were quantified using methods that selectively titrate residual H^+ sites in metal-exchanged zeolites [66–68]. The titration method involves saturation of zeolites (~0.03 to 0.05 g) with NH_3 at 433 K (500 ppm, balance He, 2 h, 350 mL min^{-1}), followed by removal of physisorbed and Cu-bound NH_3 by treatment in wet helium (2.5–3.0 % H_2O in balance He, 8 h, 350 mL min^{-1}), to selectively retain surface NH_4^+ species [66,67]. Co^{2+} ion exchange was used to quantify the fraction of total Al present as Al pairs by titrating the number of paired Al to saturation [14]. Co-SSZ-13 zeolites were prepared by ion exchange of H-SSZ-13 with an aqueous 0.25 M $Co(II)(NO_3)_2$ solution (150 mL g $catalyst^{-1}$) for 4 h at ambient conditions, not controlling the pH (pH stabilized between 3.2 and 3.6 after 4 h). Data also presented in Table S1.

2.4. Carbon monoxide temperature programmed reduction (CO-TPR)

Carbon monoxide temperature programmed reduction (CO-TPR) was performed following procedures outlined in Beutel et al., Lee et al., and Da Costa et al. [60,69,70]. The sample (~30 mg, sieved to 125 to 250 μm) was loaded into an AutoChem™II 2920 equipped with a mass spectrometer. The sample was first heated to 773 K at a rate of 9 K min^{-1} under the flow of 50 mL min^{-1} dry air (commercial grade, Indiana Oxygen Co.) and held for 2 h before cooling to room temperature. The sample was then flushed with 50 mL min^{-1} He (99.999 %, ultra high purity, Indiana Oxygen Co.) at room temperature for 2 h to flush out residual oxygen. CO-TPR was then performed under 18 mL min^{-1} flow of 5 % CO/He (standard grade, Praxair Distribution, Inc.) up to the temperature of 833 K with a ramp rate of 10 K min^{-1}. CO_2 evolution was probed using the m/z = 44 signal in the mass

spectrometer. The total CO_2 evolved was quantified by integrating the CO-TPR between 303 K and 573 K.

2.5. Fourier-Transform infrared spectroscopy (FTIR)

In situ transmission FTIR was collected on zeolite samples using a Nicolet 6700 FTIR spectrometer equipped with a liquid nitrogen-cooled mercury cadmium telluride (MCT) detector. Catalyst samples (~40 to 50 mg) were pressed into a self-supporting wafer (~2 cm in diameter) and placed in a custom-built FTIR cell [71,72]. Wafers were treated in flowing oxygen (10 % O_2/He, standard grade, Praxair Distribution, Inc.) to 673 K for 30 min and then cooled to 575 K, prior to the exposure to NO oxidation reaction gases 300 ppm NO (from 0.5 % NO/He, Praxair Distribution, Inc.), 150 ppm NO_2 (from 1 % NO_2/He, Praxair Distribution, Inc.), 10 % O_2 (from 99.999 %, ultra high purity, Matheson Tri-Gas), in balance He (99.999 %, ultra high purity, Matheson Tri-Gas). Spectra were collected with a resolution of 4 cm^{-1}, averaged over 36 scans and baseline corrected.

2.6. Steady state NO oxidation kinetic measurements

NO oxidation kinetics (rates, reaction orders, and apparent activation energies) were measured with a down-flow tubular quartz reactor with an inner diameter of 13 mm. All samples were sieved to retain 125 to 250 μm particles (W.S. Tyler No. 60 and No. 120 all-stainless-steel sieves). The temperature across the catalyst bed was measured by placing two K-type thermocouples, one touching the quartz wool above the catalyst bed and the other ~ 2 mm below the supporting glass frit. The reactor was secured within a clamshell furnace (Applied Test Systems) and leak checked by pressurizing with helium (99.999 %, ultra high purity, Indiana Oxygen Co.) to 5 psig. The standard NO oxidation feed consisted of 300 ppm NO (from 3.5 % NO/Ar, standard grade, Praxair Distribution, Inc.), 150 ppm NO_2 (from 1.0 % NO_2/Ar, standard grade, Praxair Distribution Inc.), 10 % O_2 (from 99.5 % O_2, commercial grade, Indiana Oxygen Co.) in balance N_2 (boiloff from liquid Nitrogen, Linde) The feed gases from the gas manifold were preheated by flowing through a preheater maintained at 300 °C prior to entering the main reactor to minimize axial temperature gradients, measured using the two thermocouples (typically < 5 K difference). Gas-phase concentrations of NO, NO_2, CO_2, H_2O, and N_2O were measured using a Fourier transform infrared (FTIR) analyzer (MKS Multigas™ 2030 gas-phase FTIR spectrometer). More details on the reactor set-up can be found in the Supplementary Information, Section S1.

The conversion of NO was measured according to Equation (1), where NO_{in} and NO_{out} are the concentrations of NO entering and leaving the reactor in ppm.

$$NO\ \ conversion = \frac{NO_{in} - NO_{out}}{NO_{in}} \cdot 100 \tag{1}$$

In the limit of differential conversion with product (i.e. NO_2) co-fed, the gas concentrations (NO, O_2, NO_2) and catalyst bed temperature can be assumed constant [73–78], resulting in systematic errors ranging from near zero (< 5 % conversion) to 1.2 % (20 % conversion) [73], much lower than the error from experimental repeats (typically 10 to 20 %). This allows the NO consumption rate to be calculated using the continuous stirred tank reactor (CSTR) design equation [75]:

$$-r_{overall}\left(mol_{\ NO}\ \ mol_{\ Cu}{}^{-1}\ s^{-1}\right) = \frac{NO\ \ conversion}{1000000 * mol_{Cu}} \cdot NO_{in} \cdot \dot{V}_{total} \cdot \frac{P}{RT} \tag{2}$$

where NO_{in} is the inlet NO concentration in ppm, $\dot{V}_{total}$ is the total volumetric flow rate, P is 1 atm, T is ambient temperature, and R is the gas constant. All reaction rates and kinetic parameters reported were collected in the limit of differential conversion and with products co-fed.

Based on the overall NO oxidation rate ($r_{overall}$), the normalized forward rates (r_{fwd}) were reported in the form of a power rate law model. The approach to equilibrium (β) was included because the NO oxidation rates could potentially be limited by equilibrium under the relevant reaction temperatures [54].

$$r_{fwd} = r_{overall}(1 - \beta) \tag{3}$$

$$r_{fwd} = Ae^{\frac{-E_A}{RT}}[NO]^a[O_2]^b[NO_2]^c \tag{4}$$

$$\beta = \frac{[NO_2]}{K[NO]^2[O_2]} \tag{5}$$

With K as the equilibrium constant for the NO oxidation reaction, the value of β for all the measurements were <0.18, indicating that the reaction rates measured were sufficiently far from equilibrium. A is the pre-exponential factor (s^{-1}) and E_A the activation energy (kJ mol^{-1}). a, b, and c represent forward reaction orders with respect to NO, O_2 and NO_2 respectively. The nitrogen balance in and out of the reactor was quantitatively confirmed to be complete within < 5 % for all measurements using $(NO + NO_2)_{in}$ - $(NO + NO_2)_{out}$.

3. Results and discussion

3.1. NO oxidation kinetics

Dry NO oxidation kinetics (reaction rate, apparent activation energies, and apparent reaction orders) on samples with varying densities of Z_2Cu and ZCuOH are shown in Fig. 1. We observe that, across all samples with varying Si:Al and Z_2Cu and ZCuOH fractions, dry NO oxidation reaction rates per gram catalyst collapse onto a parabola when plotted against the ZCuOH density (Fig. 1A, Figure S1). This signifies that Brønsted acid sites and Z_2Cu do not play a significant role in dry NO oxidation. By process of elimination, this leaves ZCuOH as the species responsible, either directly or indirectly, in catalyzing dry NO oxidation. The parabolic dependence suggests that dry NO oxidation over ZCuOH is not catalyzed by single ZCuOH sites, but rather by dimeric sites formed from ZCuOH.

Our observation that Z_2Cu sites are inactive towards dry NO oxidation is consistent with Verma et al. [26], who measured no detectible dry NO oxidation on a series of Cu-SSZ-13 samples with only Z_2Cu. Further, Akter et al. [79] synthesized a series of Cu-SAPO-34 with Cu loadings between 0 and 6 wt%; they observed undetectable dry NO oxidation at low Cu loadings of 0.0 and 0.5 wt% and detectable dry NO oxidation at higher Cu loadings of 4 and 6 wt%. This is consistent with the understanding that Z_2Cu (which are NO oxidation inactive), populates first, followed by ZCuOH [13]. This lead us to conjecture that Akter et al.'s 4 and 6 Cu wt% samples likely contained enough ZCuOH sites to form the dimeric Cu necessary to catalyze dry NO oxidation. Knorpp et al. [53] also observed a similar threshold on Cu-MAZ for the stepwise partial oxidation of methane to methanol, suggesting similar active species for the two reactions.

Though we measured undetectable dry NO oxidation rates on samples with only Brønsted acids (Table S2), Loiland and Lobo [80,81] observed that Brønsted acid sites and confinement imparted by the zeolite pores can activate dry NO oxidation at low temperatures of 373 K. Because their apparent negative activation energies and reaction orders of 2 for NO and 1 for O_2 coincide with gas-phase NO oxidation kinetics [82], they proposed that the reaction mechanism is akin to that of the gas-phase and is acceler-

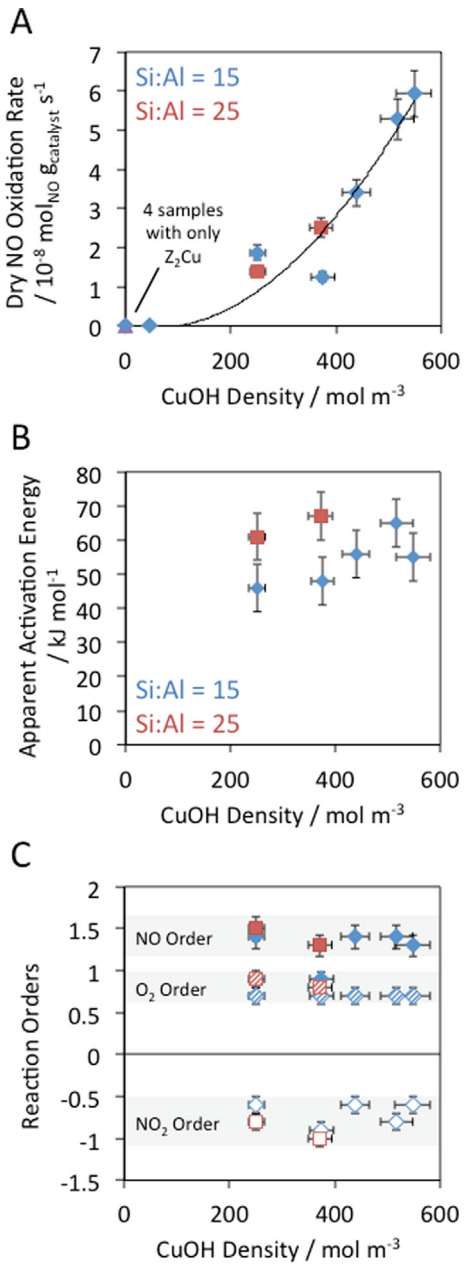

Fig. 1. (A) Dry NO oxidation rates per gram catalyst, (B) apparent activation energies, and (C) reaction orders were measured on samples with varying CuOH densities (blue diamonds, ◆, represent Si:Al = 25 and red squares, ■, represent Si:Al = 15). In (C), reaction order dependences on NO, O_2, and NO_2 are represented by filled, hatched, and hollow symbols, respectively. Dry NO oxidation reaction conditions: 300 ppm NO, 150 ppm NO_2, 10 % O_2, 550 K. Tabulated results are available in Table S2. (For interpretation of the references to colour in this figure legend, the reader is referred to the web version of this article.)

ated by pore-stabilization (by the zeolite pores) and electronic-stabilization (by Brønsted acid sites) of a N_2O_4 transition state. The negative apparent activation energies indicate that the NO oxidation rate of this zeolite-catalyzed gas-phase NO oxidation becomes more than an order of magnitude lower ($\sim 10^{-9}$ mol_{NO} g_{cat} s^{-1}) than our measured NO oxidation rates at 573 K. This is consistent with our measurements of undetectable dry NO oxidation rates on Cu-free zeolites (Table S2) and those reported by Verma et al. [26] on H-SSZ-13 (Si:Al = 4.5) and Akter et al. [79] on H-SAPO-34 ((Al + P):Si = 1.0).

In Fig. 1B and 1C, apparent activation energies and reaction orders remain constant across ZCuOH densities of 0 to 600 mol_{CuOH} m^{-3}. This suggests that that the kinetically relevant step(s) during dry NO oxidation are the same across all the samples. Akter et al. [79] reported apparent activation energies between 17 and 35 kJ mol^{-1}, which are about half of that reported in Fig. 1B. This lower apparent activation energy is an artifact from not co-feeding NO_2, which is a product that inhibits the reaction [26,31,33]. Because of this, the NO_2 concentration is not axially differential across the catalytic bed [77,78]. Once corrected [78], their apparent activation energies lie between 35 and 70 kJ mol^{-1}, consistent with our experimentally measured values between 45 and 60 kJ mol^{-1}.

On clustered Cu_xO_y, Verma et al. [26] measured apparent activation energies between 45 and 55 kJ mol^{-1}, NO orders between 1.4 and 1.5, O_2 orders between 0.8 and 0.9, and NO_2 orders between −0.7 and −0.9. These kinetic parameters are indistinguishable from our kinetic results on samples without clustered Cu_xO_y (Fig. 1B and 1C), signifying a similar reaction landscape and mechanism between our dimeric species and Verma et al.'s clustered Cu_xO_y. Diffuse reflectance UV–Visible on our series of Cu-SSZ-13 displays four peaks in the d-d transition region between 7000 and 22000 cm^{-2} (Figure S2) indicating that multi-nuclear Cu oxides indeed are present after oxidative thermal dehydration [11,83]. Because dimers and clusters both exhibit the same kinetics, it would befit to bridge the two and claim that any multi-nuclear copper oxide, no matter the size, exhibits similar reaction mechanisms. By extension, this indicates that Cu-oxide trimers, which have been proposed the play an integral role in the oxidation of methane to methanol [50–52], likely also catalyze dry NO oxidation.

3.2. Quantification of Cu-oxo sites and fraction of proximal and pairable ZCuOH

The fraction of Cu species with reactive oxygen atoms (e.g. CuO and CuO_xCu) were previously quantified from the evolution of CO_2 during CO-TPR in Cu-ZSM-5 [60,69,70]. Utilizing this technique, we performed CO-TPR in Cu-SSZ-13 with varying densities of ZCuOH (Fig. 2A). We observed that Cu-SSZ-13 with only Z_2Cu exhibit no measurable CO_2 evolution during CO-TPR, indicating that oxygen from the zeolite framework alone is unable to oxidize CO to CO_2 and that the presence of Z_2Cu does not enable the oxidation of CO to CO_2 [84]. In addition, Cu-SSZ-13 with a low ZCuOH density of 47 mol_{CuOH} m^{-3} (Si:Al = 15, CuOH:Al = 0.03) displayed no detectable CO_2 evolution, indicating that the oxygen atom in disperse monomeric ZCuOH also do not appreciably react with CO to form CO_2.

Cu-SSZ-13 with higher CuOH densities (251 to 548 mol_{CuOH} m^{-3}) displays three prominent features at 350 K, 440 K and 510 K (Fig. 2A). Using Na-Cu-ZSM-5 (Si:Al = 20, Cu wt% = 3.1), Sárkány et al. [85] observed two features at 340 K and 510 K after CO-TPR; they assigned these two features to the reduction of $[Cu-O-Cu]^{2+}$ and CuO, respectively. In contrast, Da Costa et al. [70] observed three features in their CO-TPR on Cu-ZSM-5 (Si:Al = 14, Cu:Al from 0.12 to 0.60). The reason behind this discrepancy is not clear, though it can possibly be attributed to sodium cations, the aluminum distribution within the ZSM-5, and/or the copper loading. Nonetheless, these past reports in conjunction with our CO-TPR results indicate that there indeed are different pools of reactive oxygen species. Because our CO-TPR ruled out the zeolite framework and isolated ZCuOH as potential sources of reactive oxygen species for the oxidation of CO to CO_2, we are left with dimeric Cu-oxo species as sources of reactive oxygen. In essence, we envisage that at least three pools of dimeric Cu-oxo species are responsible for the three features Fig. 2A. We postulate that the different pools of dimeric Cu-oxo species [86,87] may arise from (1) the presence of Cu-oxo species with different oxygen-

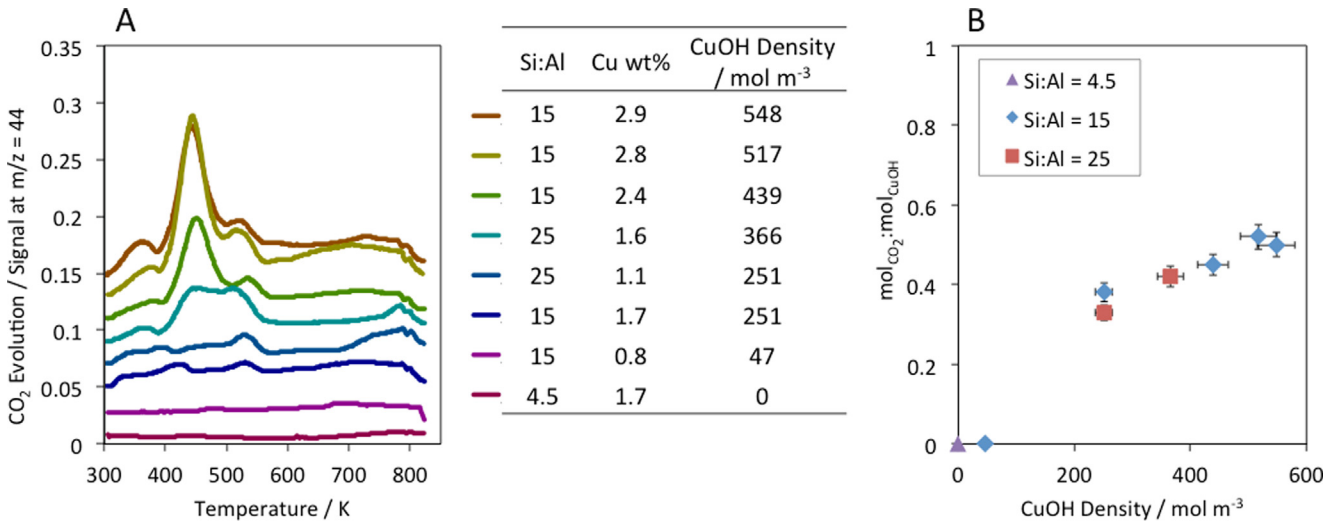

Fig. 2. (A) Carbon monoxide temperature programmed reduction (CO-TPR) profiles for a series of Cu-SSZ-13 samples with Si:Al 4.5 to 25 and CuOH densities varying from 0 to 548 mol_{CuOH} m^{-3}. (B) Total CO_2 evolved from CO-TPR between 303 and 573 K as a function of the ZCuOH density (▲ Si:Al = 4.5, ◆ Si:Al = 15, ■: Si:Al = 25).

to-Cu ratios (e.g. $[CuO_2Cu]^{2+}$, $[CuOCu]^{2+}$, $[Cu_3O_3]^{2+}$, etc.), (2) the presence of hydrogen atoms in the Cu-oxo species (e.g. $[CuO_2H_2\text{-}Cu]^{2+}$) and/or (3) different geometry arising from coordination to different anionic framework sites.

Using a statistical argument, with increasing ZCuOH density, one would expect only isolated ZCuOH at low densities, pairs of ZCuOH able to dimerize at higher densities, and trios of ZCuOH able to trimerize at even higher densities. The existence of dimeric Cu-oxo species in Cu-SSZ-13 after O_2 treatment at 723 K has been proposed to exist in samples with high Cu densities, but not on samples with low Cu densities [20–22,26,28]. Formation of $[Cu–O_2–Cu]^{2+}$ (*trans*-μ-1,2-peroxo dicopper(II)) and $[Cu–O–Cu]^{2+}$ (mono–(μ–oxo) dicopper(II)) from proximal $[CuOH]^+$ sites has been proposed based on evidence from Raman and UV–vis spectroscopy [20,21]. As such, we propose Cu dimers ($[Cu–OH_x–Cu]^{2+}$ and/or $[Cu–O_2H_x\text{-}Cu]^{2+}$, where x = 0, 1, or 2) as candidate Cu-oxo species active for dry NO oxidation.

$$[CuOH_xCu]^{2+} + CO \rightarrow 2CuH_x{}^{1+} + CO_2 \quad (6)$$

$$[CuO_2H_xCu]^{2+} + 2CO \rightarrow 2CuH_x{}^{1+} + 2CO_2 \quad (7)$$

The "H_x" (where x = 0, 1, or 2) in Equations (6) and (7) signifies that it is uncertain whether or not hydrogen atoms are present in Cu-oxo species, and if present, whether they exist as hydrides, neutral hydrogen atoms, or protons. In Equations (6) and (7), we assume that the hydrogen atoms remain neutral and Cu atoms are reduced to a 1+ oxidation state. Göltl et al. [88] recently demonstrated using density functional theory that hydroxylated Cu dimers are thermodynamically more stable than non-hydroxylated Cu dimers. Göltl et al. [86] then demonstrated using time dependent density functional theory (DFT) with spin–orbit coupling that hydroxylated Cu dimers exhibit features that better match experimental UV–Visible spectra than non-hydroxylated Cu dimers. Overall, the interaction of materials with hydrogen is not well understood. This is primarily because common techniques used to study the nature of hydrogen atoms (NMR, FTIR, Raman, etc.) are unable to detect all hydrogen atoms due to selection rules. Using neutron scattering to overcome these limitations holds promise in revealing the nature of hydrogen atoms in catalysis [89,90].

A relation between the moles of CO_2 evolved normalized per mole of ZCuOH to the ZCuOH density is observed (Fig. 2B). If Equation (6) were the dominant pathway, we would expect an asymptote at a CO_2:CuOH ratio molar ratio of 0.5. If Equation (7) were the dominant pathway, we would expect an asymptote at a CO_2:CuOH ratio molar ratio of 1.0. If both pathways contribute, the asymptote would lie between 0.5 and 1.0. Though we are unable to clearly discern between these three scenarios, it is clear that CO_2 evolution is dependent on the ZCuOH density and is independent of the presence Z_2Cu and the Brønsted acid sites.

Paolucci et al. performed Monte Carlo simulations by randomly distributing monomeric species in a volume and counting the number of species with overlapping diffusion spheres [22]. They originally utilized this simulation to understand the formation of $[(NH_3)_2Cu\text{-}O_2\text{-}Cu(NH_3)_2]^{2+}$ dimers from two $Cu^{1+}(NH_3)_2$ and O_2. From coupling experimental quantification of the fraction of pairable $Cu^{1+}(NH_3)_2$ and metadynamics calculations of the $Cu^{1+}(NH_3)_2$ energy landscape within SSZ-13, they found that $Cu^{1+}(NH_3)_2$ exhibited diffusion radii of ~0.90 nm [22].

To determine the diffusion radius of unsolvated ZCuOH, we combined the Monte Carlo simulations reported in Paolucci et al. [22] with experimental CO-TPR results (Fig. 3A). As discussed earlier, it is ambiguous whether Cu-oxo dimers speciate as $[Cu–OH_x–Cu]^{2+}$ and/or $[Cu–O_2H_x\text{-}Cu]^{2+}$. Reduction of $[Cu–OH_x–Cu]^{2+}$ with CO would produce one CO_2 (Equation (8)) whereas reduction of $[Cu–O_2H_x\text{-}Cu]^{2+}$ with CO would produce two CO_2 (Equation (9)). Using these two scenarios (Fig. 3A), we observe that the diffusion radius of dehydrated ZCuOH necessary to form $[Cu–OH_x\text{-}Cu]^{2+}$ is 0.50 nm. A diffusion radius much lower than 0.50 nm is necessary form exclusively $[Cu–O_2H_x\text{-}Cu]^{2+}$. This indicates that, when dehydrated, ZCuOH tethered to the SSZ-13 framework has a diffusion radius of at most 0.50 nm. Illustrated in Fig. 3B, dehydrated ZCuOH with a diffusion radius 0.50 nm allows access to about half of each of the two adjacent chabazite cages.

If primarily $[CuOH_xCu]^{2+}$,

$$Fraction\ of\ pairable\ CuOH = \frac{mol_{CO_2}}{mol_{CuOH}} \quad (8)$$

If primarily $[CuO_2H_xCu]^{2+}$,

$$Fraction\ of\ pairable\ CuOH = \frac{\frac{1}{2}mol_{CO_2}}{mol_{CuOH}} \quad (9)$$

3.3. Turnover rates

NO oxidation rates increase linearly with CO_2:CuOH (Fig. 4A). We interpret this as an indication that dimeric Cu-oxo species with

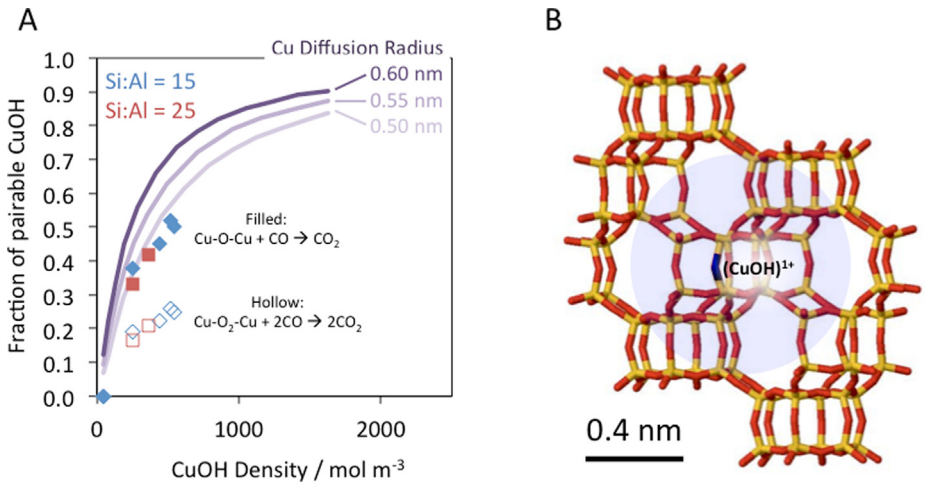

Fig. 3. (A) The fraction of paired ZCuOH quantified by CO-TPR for Si:Al = 15 (blue diamonds, ◆) and Si:Al = 25 (red squares, ■) plotted against the CuOH density. The three purple lines represent the fraction of moieties with overlapping diffusion spheres of 0.50, 0.55, 0.60 nm (data from Paolucci et al. [22]). (B) Representation of the diffusion radius accessible by ZCuOH after dehydration. The light blue sphere around $(CuOH)^{1+}$ signify a maximum diffusion radii of 0.50 nm. (For interpretation of the references to colour in this figure legend, the reader is referred to the web version of this article.)

reactive oxygen probed via CO-TPR are the active site for NO oxidation. However, because the different pools of Cu-oxo species have different reactivities with CO (as indicated by the different temperatures at which CO_2 is formed during CO-TPR), we presume that the different pools of Cu-oxo species would also exhibit different reactivities towards dry NO oxidation. If this were true, the overall turnover rate (TOR) would be a weighted average of the turnover rates of each distinct pool of Cu-oxo species (Equation (10)). We denote the Cu-oxo species that evolve CO_2 at 350 K, 440 K, and 510 K, (Fig. 3A) as Pool 1, Pool 2, and Pool 3, respectively. The fraction, f_x (x = 1, 2, 3), of the three Cu-oxo pools was quantified by fitting the CO-TPR to three Gaussian curves (Fig. 5).

$$TOR_{experimental} = f_1 TOR_1 + f_2 TOR_2 + f_3 TOR_3 \quad (10)$$

$$\min \sum \left| \Delta (TOR_{experimental} - TOR_{predicted}) \right| \quad (11)$$

To determine the turnover rates of the individual pools of Cu-oxo species, we equated the experimentally measured dry NO oxidation rate (normalized to the total mols of CuOH) to the summation of the product of each pool's fraction and corresponding turnover rate (Equation (10)). Using our six samples with varying CuOH density (Fig. 3A and 5), we attain a system of 6 linear equations and three unknowns. Using reasonable initial guesses (TOR_1, TOR_2, TOR_3) and the Generalized Reduced Gradient (GRG) algorithm to converge the initial guesses until the sum of the absolute values of the differences between the experimental TOR and predicted TOR are minimized (Equation (11)), we discovered two local minima (Table 1). The two local minima signify-two plausible solutions for the TORs of each of the three pools of Cu-oxo species (Table 1). Section S5 provides all the initial guesses and bar charts comparing the experimental and predicted NO oxidation rates.

In both cases (Table 1), Pool 1 exhibited the highest turnover rate, followed by the Pool 2, then Pool 3. The first pool of Cu-oxo species is predicted to exhibit turnover rates 2 to 30 times faster than the third pool of Cu-oxo species. This trend indicates that the Cu-oxo moieties able to evolve CO_2 at lower temperatures are more active than Cu-oxo moieties that evolve CO_2 at elevated temperatures for dry NO oxidation. Following a Sabatier argument [91], we conjecture that Cu-oxo species that bind CO too strong would oxidize CO at higher temperatures, and thus also strongly bind NO and thus exhibit lower dry NO oxidation rates. Conversely, Cu-oxo species that bind CO weaker would oxidize CO at lower

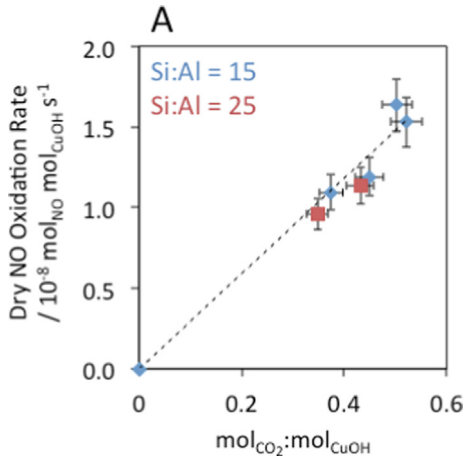

Fig. 4. NO oxidation rates normalized per mol of ZCuOH as a function of moles of CO_2 evolved normalized per mole ZCuOH.

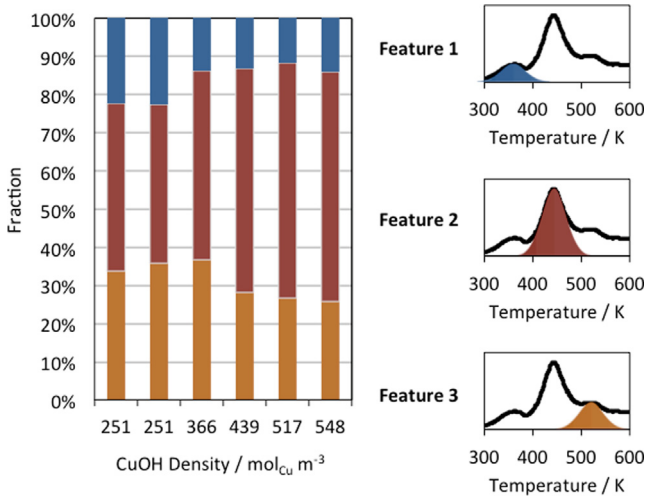

Fig. 5. Fractions (f_1, f_2, f_3) of the three CO-TPR features at 350 K, 440 K, and 510 K quantified by fitting CO-TPR to three Gaussian curves.

Table 1
Turnover rates of each pool of Cu-oxo species determined from minimizing the residuals between experimental and predicted turnover rates. Two plausible solutions (located at two local minima) were discovered, with Local Minimum 2 exhibiting the lowest discrepancy between experimental and predicted total rates.

	TOR_1/s^{-1}	TOR_2/s^{-1}	TOR_3/s^{-1}	$\Sigma\lvert\Delta TOR_x\rvert/s^{-1}$
Local Minimum 1	3.97	2.54	2.25	0.24
Local Minimum 2	5.73	3.58	0.19	0.12

temperatures, and thus also bind NO more weakly and exhibit higher dry NO oxidation rates. With even weaker CO or NO binding, we predict the dry NO oxidation rate to reach a maximum then start decreasing.

3.4. Impact of NH_3 and H_2O

From an industrial standpoint, maximizing the Cu-oxo pool that exhibits the highest turnover rate for reactions of interest is economically favorable. Because Cu-zeolites are promising for reactions that involve partial pressures of solvating species such as H_2O or NH_3, it is pertinent to also discuss the impact of H_2O and NH_3 on Cu-oxo formation. Because much of this chemistry is still unclear, we present evidence from the literature then discuss potential implications for partial methane oxidation.

Consistent with our results, Villamaina et al. [92] used low temperature CO oxidation to probe dimeric Cu-oxo species and demonstrated that, in the absence of dioxygen (O_2), Cu-oxo species are formed only from ZCuOH. Further, when NH_3 was presaturated, increased CO oxidation was observed, presumably due to the increased fraction of Cu-oxo species formed due to an increased ZCuOH diffusion sphere [92]. In a follow-up study, Hu et al. [93] also demonstrated that exposing NH_3-saturated Cu-SSZ-13 to H_2O further increased CO oxidation rates. To explain this observation, Hu et al. [93] proposed a two-step reaction. The first thermodynamically-limited step involves H_2O converting a fraction of NH_3-saturated Z_2Cu to ZCuOH and ZH (Brønsted acid site). Because this reaction is thermodynamically-limited, the majority of the formed ZCuOH and ZH immediately revert back to Z_2Cu. The second step involves the participation of the miniscule remaining fraction of the ZCuOH in CO oxidation, resulting in an observed increase in the CO oxidation rate.

Similar to Hu et al. [93], Shih [94] proposed that exposure of dehydrated Z_2Cu to either aqueous H_2O or H_2O vapor is able to convert Z_2Cu to ZCuOH and ZH; the generated ZH was quantified via selective titration with NH_3 [67]. Density functional theory (DFT) calculations by Hu et al. [93], however, suggests that converting Z_2Cu to ZCuOH in the absence of NH_3 is more kinetically challenging compared to in the presence of NH_3. A couple earlier studies also reported the intriguing interconversion of Z_2Cu and ZCuOH. Luo et al. [95] observed an increase of NH_3 coordinated to Lewis acidic Cu sites and decrease in Brønsted acidic ZH after hydrothermal treatments of Cu-SSZ-13; they attributed this observation to the interconversion of Z_2Cu to ZCuOH during hydrothermal steaming. Song et al. [96] also observed the interconversion of Z_2Cu to ZCuOH during hydrothermal steaming and used Co^{2+} titration [104] of paired framework Al to demonstrate that the increase in ZCuOH was not due to a redistribution of framework Al. Since H_2O is the oxidant for the continuous production of methanol from methane over Cu-SSZ-13 [45,46,97], a robust understanding of the impact of H_2O on Cu speciation would shed light into not only methane-to-methanol, but other reactions involving H_2O.

3.5. Proposed NO oxidation reaction mechanism and relevant steps

We propose an atomically balanced reduction–oxidation catalytic mechanism based on the aforementioned kinetic, UV–Visible, and CO-TPR results (Fig. 6). Starting from hydrated Cu-SSZ-13, there are at least three pathways to form the active Cu-oxo sites: two adjacent ZCuOH species can either (1) dimerize via a partial dehydration reaction to $[Cu–O_2H_2–Cu]^{2+}$, (2) react with dioxygen to $[Cu–O–Cu]^{2+}$, or (3) autoreduce via a still-debated mechanism [12,98,99] during dehydration in inert or under vacuum to form two proximal Cu^{1+}. A recent contribution by Göltl et al. [88] predicted using density functional theory (DFT) that upon exposure to dioxygen at elevated temperatures (up to 800 K), hydroxylated Cu dimers are more stable than non-hydroxolated Cu dimers. Within the framework of our proposed dry NO oxidation mechanism and DFT results by Göltl et al. [88], we would expect that $[Cu–O_2H_2–Cu]^{2+}$ species formed after partial dehydration of proximal ZCuOH (Pathway (1)) would dominate prior to exposure to our dry NO oxidation gas feed.

Summarizing the cycle starting from $[Cu–O–Cu]^{2+}$, Step 1 occurs when NO reacts with $[Cu–O–Cu]^{2+}$ to form $[Cu–ONO–Cu]^{2+}$. Step 2 occurs when $[Cu–ONO–Cu]^{2+}$ releases NO_2 and $2Cu^{1+}$. It is at this stage when pairs of Cu^{1+} formed from autoreduction or reduction of partially-dehydrated $[Cu–O_2H_2–Cu]^{2+}$ by NO enter the catalytic cycle. In Step 3, the $2Cu^{1+}$ are oxidized by dioxygen to form $[Cu–O_2–Cu]^{2+}$. In Step 4, $[Cu–O_2–Cu]^{2+}$ reacts with NO with form $[Cu–O_2NO–Cu]^{2+}$, followed by release of NO_2 in Step 5 to complete the cycle with $[Cu–O–Cu]^{2+}$.

The NO oxidation mechanism by Fahami et al. [100] and Ruggeri et al. [101] proposes that $[Cu–O–Cu]^{2+}$ decomposes into Cu^{+} and $Cu^{2+}ONO$ upon adsorption of NO, whereas we proposed that the dimer remains intact prior to cleavage of the dimer and desorption of NO_2. Upon desorption of NO_2, both mechanisms propose that Cu is reduced to bare Cu^{+}. Whereas Fahami et al. [100] and Ruggeri et al. [101] regenerates $[Cu–O–Cu]^{2+}$ by reacting $2Cu^{+}$ with $½O_2$, we proposed that $2Cu^{+}$ reacts with O_2 to form $[Cu–O_2–Cu]^{2+}$, which converts to $[Cu–O–Cu]^{2+}$ after converting an additional NO to NO_2. The mechanism by Fahami et al. [100] and Ruggeri et al. [101] do include potential impacts of trace water, proposing that H_2O can (1) react with the $Cu^{2+}ONO$ intermediate to form $Cu^{2+}OH$ and gaseous nitrous acid (HONO), and (2) decompose $[Cu–O–Cu]^{2+}$ to $2Cu^{2+}OH$.

Equations (12) through (16) are rate laws derived for the proposed catalytic cycle (Fig. 6) assuming that the forward rate of each of the five elementary steps are rate limiting, respectively, while all other steps are quasi-equilibrated. Assuming that all pre-exponential factors (k_i), rate constants (K_i), and pressures (P_{NO}, P_{O_2}, P_{NO_2}) are unity (set to a value of 1), we performed a sensitivity analysis by varying each reaction pressure of interest (P_{NO}, P_{O_2}, or P_{NO_2}) to determine how the NO oxidation rate and its corresponding reaction order changes with within an arbitrary pressure range of 10^{-9} to 10^{9}. Results of this sensitivity analysis are tabulated in Table 2 and plotted in Figures S5 to S9 in Section S6.

$$r_1 = \frac{k_1 P_{O_2}}{1 + \frac{P_{NO_2}^2}{K_2K_3K_4K_5P_{NO}} + \frac{P_{NO_2}^2}{K_3K_4K_5P_{NO}} + \frac{P_{NO_2}}{K_4K_5P_{NO}} + \frac{P_{NO_2}}{K_5}} \tag{12}$$

$$r_2 = \frac{K_1 k_2 P_{NO} P_{O_2}}{1 + K_1 P_{O_2} + \frac{P_{NO_2}}{K_5} + \frac{P_{NO_2}}{K_4K_5P_{NO}} + \frac{P_{NO_2}^2}{K_3K_4K_5P_{NO}}} \tag{13}$$

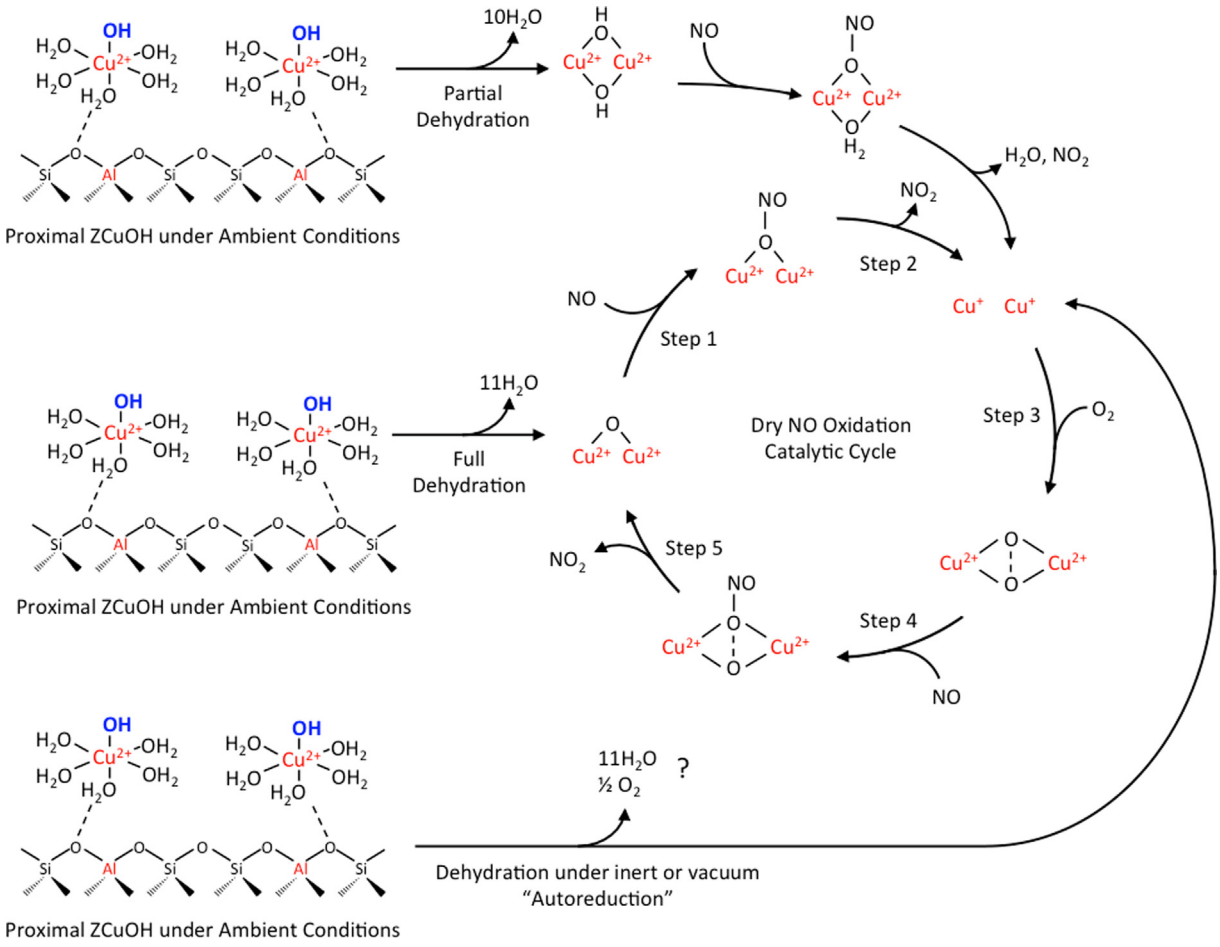

Fig. 6. Proposed dry NO oxidation mechanism over two proximal ZCuOH sites. Under ambient conditions the two proximal ZCuOH are hydrated and release 11 or 10 H_2O molecules upon full or partial dehydration during dimerization to $[Cu–O–Cu]^{2+}$ and $[Cu–O_2H_2–Cu]^{2+}$ dimer active site for dry NO oxidation. The zeolite framework is not shown for clarity in the dry NO oxidation mechanism; throughout the mechanism the Cu are dehydrated and electrostatically tethered to the zeolite framework.

Table 2
Summary of predicted NO, O_2, and NO_2 reaction orders from the sensitivity analysis compared to the experimentally measured reaction orders.

Rate Limiting Step	NO Order		O_2 order		NO_2 order		Plausible RLS?
	Low P	High P	Low P	High P	Low P	High P	
1	1	0	1	1	0	−2	No
2	2	1	1	0	0	−2	Yes
3	2	0	1	0	0	−1	Yes
4	2	1	1	0	0	−2	Yes
5	1	−1	1	0	0	−1	No
Experimental Reaction Orders	1.0 to 1.5		0.7 to 0.9		−0.1 to −0.6		

$$r_3 = \frac{K_1K_2k_3P_{NO}P_{O_2}}{1 + K_1P_{O_2} + K_1K_2P_{O_2}P_{NO} + \frac{P_{NO_2}}{K_5} + \frac{P_{NO_2}}{K_4K_5P_{NO}}} \quad (14)$$

$$r_4 = \frac{K_1K_2K_3k_4\frac{P_{NO}^2P_{O_2}}{P_{NO_2}}}{1 + K_1P_{O_2} + K_1K_2P_{O_2}P_{NO} + K_1K_2K_3\frac{P_{O_2}P_{NO}}{P_{NO_2}} + \frac{P_{NO_2}}{K_5}} \quad (15)$$

$$r_5 = \frac{K_1K_2K_3K_4k_5\frac{P_{NO}P_{O_2}}{P_{NO_2}}}{1 + K_2P_{O_2} + K_1K_2P_{NO}P_{O_2} + K_1K_2K_3\frac{P_{NO}P_{O_2}}{P_{NO_2}} + K_1K_2K_3K_4\frac{P_{NO}^2P_{O_2}}{P_{NO_2}}} \quad (16)$$

Comparing the predicted reaction orders to the experimentally measured reaction orders (Fig. 1C, Table S2), steps 1 (O_2 adsorption) and 5 (NO_2 desorption) cannot be the rate-limiting step. Further, Verma et al. [26] reported in situ X-ray absorption near edge spectroscopy (XANES) and didn't observe significant pre-edge features typical of Cu^{1+}, which suggests that Step 3 is not the rate limiting step. This leaves steps 2 and 4 as plausible rate limiting steps. These remaining plausible rate limiting steps are the desorption of NO_2 from $(Cu^{2+})_2ONO$ to $2Cu^{2+}$ (Step 2) and reaction between $(Cu^{2+})_2O_2$ and NO to form $(Cu^{2+})_2O_2NO$ (step 4).

In situ FTIR spectroscopy was used to detect surface species on Cu-SSZ-13 under NO oxidation reaction conditions. Fig. 7 compares in situ FTIR spectra of Cu-SSZ-13 with measurable (Si:Al = 15, Cu:

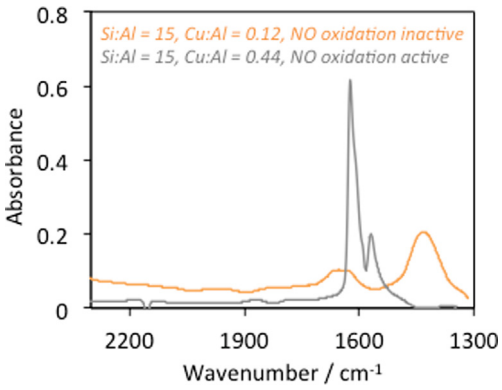

Fig. 7. In situ FTIR spectra on Si:Al = 15, Cu:Al = 0.44 (predominantly ZCuOH, measurable NO oxidation reactivity, grey) and Si:Al = 15, Cu:Al = 0.12 (only Z_2Cu, no detectable NO oxidation activity, orange) collected under NO oxidation reaction conditions (300 ppm NO, 150 ppm NO_2, and 10 % O_2 in balance He at 523 K). (For interpretation of the references to colour in this figure legend, the reader is referred to the web version of this article.)

Al = 0.44, CuOH density = 548 mol m^{-3}) and non-measurable (Si:Al = 15, Cu:Al = 12, CuOH density = 47 mol m^{-3}) dry NO oxidation rates. We observe the presence of three distinct peaks at 1567, 1601 and 1626 cm^{-1} on Cu-SSZ-13 with detectable dry NO oxidation. The feature at 1567 cm^{-1} was previously assigned to N—O stretching vibrations in monodentate nitrates while the features at 1601 and 1626 cm^{-1} were ascribed to bridged/bidentate nitrates [101–106]. If these monodendate and bidendate nitrates were the most abundant reaction intermediate, then Step 5 of the catalytic mechanism (Fig. 6) would have been the rate limiting step – a step that has been experimentally ruled out from our rate law analysis and kinetics (Table 2). As such, we posit that the nitrates observed in in situ FTIR under reaction conditions are an abundant spectator species that do not directly participate in the reaction and/or just capture the fleeting presence of nitrates formed and consumed during dry NO oxidation.

4. Conclusions and outlook

Utilizing Cu-SSZ-13 with nominally monomeric Cu sites (Z_2Cu and ZCuOH), we first confirmed that monomeric Z_2Cu, previously reported to be inactive for NO oxidation, indeed exhibited no detectable dry NO oxidation rates. A parabolic dependence of the dry NO oxidation rate when plotted against the ZCuOH density suggested that dimeric Cu-oxo species, formed from two proximal ZCuOH, are likely the active sites for dry NO oxidation. Coupling the quantification of the number of Cu-oxo dimers (from CO-TPR) with Monte Carlo simulations from Paolucci et al. [22], we found that the maximum diffusion radii of dehydrated ZCuOH is 0.50 nm, consistent with the diffusion radii predicted by *ab-initio* molecular dynamic simulations on monomeric Cu free of H_2O ligands [13]. Taken together, this evidence indicates that dehydrated ZCuOH moieties with overlapping diffusion spheres are able to dimerize and are active for dry NO oxidation.

More notably, we demonstrated that dry NO oxidation rates over Cu-SSZ-13 catalysts can be deconstructed into three distinct pools of Cu-oxo active sites, each with different CO reduction temperatures, each exhibiting different turnover rates for dry NO oxidation. The most active Cu-oxo species exhibited dry NO oxidation rates 2 to 30 times faster than the least active pool of Cu-oxo species. Although the precise structural and electronic nature of these pools of Cu-oxo species are still unclear, it does beg to question how these pools impact other oxidation chemistries such as methane upgrading (to methanol, dimethyl ether, etc.), CO oxidation, NO decomposition, the partial oxidation of aromatics, among others.

This fundamental understanding of site requirements will aid in devising strategies for more efficient catalysts. By maximizing the pools of active sites that exhibit the highest turnover rate, one can achieve increased reaction rates while utilizing the same amount of Cu. Broadly, this study also demonstrates the value in using kinetics, far from equilibrium, and complementary characterization tools to characterize pools of active sites, turnover rates, and reaction mechanisms.

Data availability

Data will be made available on request.

Declaration of Competing Interest

The authors declare that they have no known competing financial interests or personal relationships that could have appeared to influence the work reported in this paper.

Acknowledgements

We acknowledge financial support provided by the National Science Foundation GOALI program under award number 1258715-CBET, the U.S. Department of Energy Vehicle Technologies Program under contract number DE-EE0003977, and by Cummins, Inc. We also acknowledge the researchers in the Cummins Catalyst Technology Team for fruitful discussions. We thank SACHEM, Inc., for providing the organic structure directing agent used to synthesize SSZ-13.

Appendix A. Supplementary material

Supplementary data to this article can be found online at https://doi.org/10.1016/j.jcat.2022.08.005.

References

[1] S. Brandenberger, O. Kröcher, A. Tissler, R. Althoff, The state of the art in selective catalytic reduction of NO_x by ammonia using metal-exchanged zeolite catalysts, Catalysis Reviews 50 (4) (2008) 492–531, https://doi.org/10.1080/01614940802480122.
[2] J.H. Kwak, D. Tran, S.D. Burton, J. Szanyi, J.H. Lee, C.H.F. Peden, Effects of hydrothermal aging on NH_3-SCR reaction over Cu/zeolites, J. Catal. 287 (2012) 203–209, https://doi.org/10.1016/j.jcat.2011.12.025.
[3] J.D. Albarracin-Caballero, I. Khurana, J.R. Di Iorio, A.J. Shih, J.E. Schmidt, M. Dusselier, M.E. Davis, A. Yezerets, J.T. Miller, F.H. Ribeiro, R. Gounder, Structural and kinetic changes to small-pore Cu-zeolites after hydrothermal aging treatments and selective catalytic reduction of NO_x with ammonia, React. Chem. Eng. 2 (2) (2017) 168–179, https://doi.org/10.1039/C6RE00198J.
[4] I. Bull, W. Xue, P. Burk, R.S. Boorse, W.M. Jaglowski, G.S. Koermer, A. Moini, J.A. Patchett, J.C. Dettling, M.T. Claude, United State Patent No: 7,601,662 B2, 2009.
[5] U. Deka, A. Juhin, E.A. Eilertsen, H. Emerich, M.A. Green, S.T. Korhonen, B.M. Weckhuysen, A.M. Beale, Confirmation of Isolated Cu^{2+} Ions in SSZ-13 Zeolite as Active Sites in NH_3-Selective Catalytic Reduction, J. Phys. Chem. C. 116 (2012) 4809–4818, https://doi.org/10.1021/jp212450d. http://pubs.acs.org/doi/abs/10.1021/jp212450d.
[6] S.T. Korhonen, D.W. Fickel, R.F. Lobo, M. Weckhuysen, A.M. Beale, Isolated Cu^{2+} ions: active sites for selective catalytic reduction of NO, Chem. Commun. 47 (2011) 800–802, https://doi.org/10.1039/c0cc04218h.
[7] S.A. Bates, A.A. Verma, C. Paolucci, A.A. Parekh, T. Anggara, A. Yezerets, W.F. Schneider, J.T. Miller, W.N. Delgass, F.H. Ribeiro, Identification of the active Cu site in standard selective catalytic reduction with ammonia on Cu-SSZ-13, J. Catal. 312 (2014) 87–97, https://doi.org/10.1016/j.jcat.2014.01.004.
[8] J.-S. McEwen, T. Anggara, W.F. Schneider, V.F. Kispersky, J.T. Miller, W.N. Delgass, F.H. Ribeiro, Integrated operando X-ray absorption and DFT characterization of Cu–SSZ-13 exchange sites during the selective catalytic reduction of NO_x with NH_3, Catal. Today. 184 (2012) 129–144, https://doi.org/10.1016/j.cattod.2011.11.037.
[9] J. Hun Kwak, H. Zhu, J.H. Lee, C.H.F. Peden, J. Szanyi, Two different cationic positions in Cu-SSZ-13?, Chem Commun. (Camb). 48 (2012) 4758–4760, https://doi.org/10.1039/c2cc31184d.

[10] E. Borfecchia, K.A. Lomachenko, F. Giordanino, H. Falsig, P. Beato, A.V. Soldatov, S. Bordiga, C. Lamberti, Revisiting the nature of Cu sites in the activated Cu-SSZ-13 catalyst for SCR reaction, Chem. Sci. 6 (2015) 548–563, https://doi.org/10.1039/c4sc02907k.
[11] F. Giordanino, P.N.R. Vennestrøm, L.F. Lundegaard, F.N. Stappen, S. Mossin, P. Beato, S. Bordiga, C. Lamberti, Characterization of Cu-exchanged SSZ-13: a comparative FTIR, UV-Vis, and EPR study with Cu-ZSM-5 and Cu-β with similar Si/Al and Cu/Al ratios, Dalton Trans. 42 (2013) 12741–12761, https://doi.org/10.1039/c3dt50732g.
[12] F. Gao, N.M. Washton, Y. Wang, M. Kollár, J. Szanyi, C.H.F. Peden, Effects of Si/Al ratio on Cu/SSZ-13 NH_3-SCR catalysts: implications for the active Cu species and the roles of Brønsted acidity, J. Catal. 331 (2015) 25–38, https://doi.org/10.1016/j.jcat.2015.08.004.
[13] C. Paolucci, A.A. Parekh, I. Khurana, J.R. Di Iorio, H. Li, J.D. Albarracin Caballero, A.J. Shih, T. Anggara, W.N. Delgass, J.T. Miller, F.H. Ribeiro, R. Gounder, W.F. Schneider, Catalysis in a cage: condition-dependent speciation and dynamics of exchanged Cu cations in SSZ-13 zeolites, J. Am. Chem. Soc. 138 (2016) 6028–6048, https://doi.org/10.1021/jacs.6b02651.
[14] J.R. Di Iorio, R. Gounder, Controlling the isolation and pairing of aluminum in chabazite zeolites using mixtures of organic and inorganic structure-directing agents, Chem. Mater. 28 (2016) 2236–2247, https://doi.org/10.1021/acs.chemmater.6b00181.
[15] F. Gao, E.D. Walter, M. Kollar, Y. Wang, J. Szanyi, C.H.F. Peden, Understanding ammonia selective catalytic reduction kinetics over Cu/SSZ-13 from motion of the Cu ions, J. Catal. 319 (2014) 1–14, https://doi.org/10.1016/j.jcat.2014.08.010.
[16] T.V.W. Janssens, H. Falsig, L.F. Lundegaard, P.N.R. Vennestrøm, S. Rasmussen, P.G. Moses, F. Giordanino, E. Borfecchia, K.A. Lomachenko, C. Lamberti, S. Bordiga, A. Godiksen, S. Mossin, P. Beato, A consistent reaction scheme for the selective catalytic reduction of nitrogen oxides with ammonia, ACS Catal. 5 (2015) 2832–3845, https://doi.org/10.1021/cs501673g.
[17] Y.J. Kim, J.K. Lee, K.M. Min, S.B. Hong, I.S. Nam, B.K. Cho, Hydrothermal stability of CuSSZ13 for reducing NO_x by NH_3, J. Catal. 311 (2014) 447–457, https://doi.org/10.1016/j.jcat.2013.12.012.
[18] C. Paolucci, J.R. Di Iorio, W.F. Schneider, R. Gounder, Solvation and Mobilization of Copper Active Sites in Zeolites by Ammonia: Consequences for the Catalytic Reduction of Nitrogen Oxides (2020). doi:10.1021/acs.accounts.0c00328.
[19] S. Grundner, W. Luo, M. Sanchez-Sanchez, J.A. Lercher, Synthesis of single-site copper catalysts for methane partial oxidation, Chem. Commun. 52 (2016) 2553–2556, https://doi.org/10.1039/C5CC08371K.
[20] D.K. Pappas, E. Borfecchia, M. Dyballa, I.A. Pankin, K.A. Lomachenko, A. Martini, M. Signorile, S. Teketel, B. Arstad, G. Berlier, S. Bordiga, U. Olsbye, K.P. Lillerud, S. Svelle, P. Beato, D.K. Pappas, E. Borfecchia, M. Dyballa, I.A. Pankin, K.A. Lomachenko, C. Lamberti, S. Bordiga, U. Olsbye, K.P. Lillerud, S. Svelle, P. Beato, Methane to methanol: structure-activity relationships for Cu-CHA, J. Am. Chem. Soc. 139 (2017) 14961–14975, https://doi.org/10.1021/jacs.7b06472.
[21] B. Ipek, M.J. Wulfers, H. Kim, F. Göltl, I. Hermans, J.P. Smith, K.S. Booksh, C.M. Brown, R.F. Lobo, Formation of $[Cu_2O_2]^{2+}$ and $[Cu_2O]^{2+}$ towards C-H Bond Activation in Cu-SSZ-13 and Cu-SSZ-39, ACS Catal. 7 (2017) 4291–4303, https://doi.org/10.1021/acscatal.6b03005.
[22] C. Paolucci, I. Khurana, A.A. Parekh, S. Li, A.J. Shih, H. Li, J.R. Di Iorio, J.D. Albarracin-Caballero, A. Yezerets, J.T. Miller, W.N. Delgass, F.H. Ribeiro, W.F. Schneider, R. Gounder, Dynamic multinuclear sites formed by mobilized copper ions in NO_x selective catalytic reduction, Science 357 (6354) (2017) 898–903, https://doi.org/10.1126/science.aan5630.
[23] F. Gao, D. Mei, Y. Wang, J. Szanyi, C.H.F. Peden, Selective catalytic reduction over Cu/SSZ-13: linking homo- and heterogeneous catalysis, J. Am. Chem. Soc. 139 (2017) 4935–4942, https://doi.org/10.1021/jacs.7b01128.
[24] C. Liu, H. Kubota, T. Toyao, Z. Maeno, K.I. Shimizu, Mechanistic insights into the oxidation of copper(I) species during NH_3-SCR over Cu-CHA zeolites: a DFT study, Catal Sci. Technol. 10 (2020) 3586–3593, https://doi.org/10.1039/d0cy00379d.
[25] A. Martini, C. Negri, L. Bugarin, G. Deplano, R.K. Abasabadi, K.A. Lomachenko, T.V.W. Janssens, S. Bordiga, G. Berlier, E. Borfecchia, Assessing the infuence of zeolite composition on oxygen-bridged diamino dicopper(II) complexes in Cu-CHA DeNO$_x$ catalysts by machine learning-assisted X-ray absorption spectroscopy, J. Phys. Chem. Lett. 13 (2022) 6164–6170, https://doi.org/10.1021/acs.jpclett.2c01107.
[26] A.A. Verma, S.A. Bates, T. Anggara, C. Paolucci, A.A. Parekh, K. Kamasamudram, A. Yezerets, J.T. Miller, W.N. Delgass, W.F. Schneider, F.H. Ribeiro, NO oxidation: A probe reaction on Cu-SSZ-13, J. Catal. 312 (2014) 179–190, https://doi.org/10.1016/j.jcat.2014.01.017.
[27] A.J. Shih, J.M. González, I. Khurana, L.P. Ramírez, A. Peña L., A. Kumar, A.L. Villa, Influence of ZCuOH, Z_2Cu, and extraframework Cu_xO_y species in Cu-SSZ-13 on N_2O formation during the selective catalytic reduction of NO_x with NH_3, ACS Catal. 11 (16) (2021) 10362–10376, https://doi.org/10.1021/acscatal.1c01871.
[28] F. Gao, E.D. Walter, E.M. Karp, J. Luo, R.G. Tonkyn, J.H. Kwak, J. Szanyi, C.H.F. Peden, Structure–activity relationships in NH_3-SCR over Cu-SSZ-13 as probed by reaction kinetics and EPR studies, J. Catal. 300 (2013) 20–29, https://doi.org/10.1016/j.jcat.2012.12.020.
[29] K. Rahkamaa-Tolonen, T. Maunula, M. Lomma, M. Huuhtanen, R.L. Keiski, The effect of NO_2 on the activity of fresh and aged zeolite catalysts in the NH_3-SCR reaction, Catal. Today. 100 (2005) 217–222, https://doi.org/10.1016/j.cattod.2004.09.056.
[30] A.M. Beale, F. Gao, I. Lezcano-Gonzalez, C.H.F. Peden, J. Szanyi, Recent advances in automotive catalysis for NO_x emission control by small-pore microporous materials, Chem. Soc. Rev. 44 (2015) 7371–7405, https://doi.org/10.1039/C5CS00108K.
[31] M.P. Ruggeri, N. Isabella, E. Tronconi, Experimental study of the NO oxidation to NO_2 Over metal promoted zeolites aimed at the identification of the standard SCR rate determining step, Top. Catal. 56 (2013) 109–113, https://doi.org/10.1007/s11244-013-9937-0.
[32] M. Schwidder, S. Heikens, A. De Toni, S. Geisler, M. Berndt, A. Brückner, W. Grünert, The role of NO_2 in the selective catalytic reduction of nitrogen oxides over Fe-ZSM-5 catalysts: Active sites for the conversion of NO and of NO/NO_2 mixtures, J. Catal. 259 (2008) 96–103, https://doi.org/10.1016/j.jcat.2008.07.014.
[33] P.S. Metkar, V. Balakotaiah, M.P. Harold, Experimental and kinetic modeling study of NO oxidation: Comparison of Fe and Cu-zeolite catalysts, Catal. Today. 184 (2012) 115–128, https://doi.org/10.1016/j.cattod.2011.11.032.
[34] M. Colombo, I. Nova, E. Tronconi, Detailed kinetic modeling of the NH_3–NO/NO_2 SCR reactions over a commercial Cu-zeolite catalyst for Diesel exhausts after treatment, Catal. Today. 197 (2012) 243–255, https://doi.org/10.1016/j.cattod.2012.09.002.
[35] J.M. González, A.L. Villa, High Temperature SCR Over Cu-SSZ-13 and Cu-SSZ-13 and Fe-SSZ-13: Activity of Cu^{2+} and $[CuOH]^{1+}$ Sites and the Apparent Promoting Effect of Adding Fe into Cu-SSZ-13 Catalyst, Catal. Letters. 151 (2021) 3011–3019, https://doi.org/10.1007/s10562-021-03550-7.
[36] H. Lee, R.J.G. Nuguid, S.W. Jeon, H.S. Kim, K.H. Hwang, O. Kröcher, D. Ferri, D. H. Kim, In situ spectroscopic studies of the effect of water on the redox cycle of Cu ions in Cu-SSZ-13 during selective catalytic reduction of NO_x, Chem. Commun. 58 (2022) 6610–6613, https://doi.org/10.1039/d2cc01786e.
[37] N. Ottinger, Y. Xi, C. Keturakis, Z. Liu, Impact of water vapor on the performance of a Cu-SSZ-13 catalyst under simulated diesel exhaust conditions, SAE Int J. Adv. Curr. Pr. Mobil. 3 (2021) 2872–2877, https://doi.org/10.4271/2021-01-0577.
[38] L. Ma, Z. Li, H. Zhao, T. Zhang, N. Yan, J. Li, Understanding the Water Effect for Selective Catalytic Reduction of NO_x with NH_3 over Cu-SSZ-13 Catalysts, ACS EST Engg (2022) 2022, https://doi.org/10.1021/acsestengg.2c00068.
[39] M. Iwasaki, Mechanistic Aspect of NO-NH_3-O_2 Reacting System, in: I. Nova, E. Tronconi (Eds.), Urea-SCR Technol. DeNOx After Treat. Diesel Exhausts, Springer, New York, New York, NY, 2014, pp. 221–246, https://doi.org/10.1007/978-1-4899-8071-7_8.
[40] L. Olsson, H. Sjövall, R.J. Blint, Detailed kinetic modeling of NO_x adsorption and NO oxidation over Cu-ZSM-5, Appl. Catal. B Environ. 87 (2009) 200–210, https://doi.org/10.1016/j.apcatb.2008.09.007.
[41] T. Selleri, F. Gramigni, I. Nova, E. Tronconi, NO oxidation on Fe- and Cu-zeolites mixed with BaO/Al_2O_3: free oxidation regime and relevance for the NH_3-SCR chemistry at low temperature, Appl. Catal. B Environ. 225 (2018) 324–331, https://doi.org/10.1016/j.apcatb.2017.11.068.
[42] K. Khivantsev, J.-H. Kwak, N.R. Jaegers, I. Koleva, G. Vayssilov, M.A. Derewinski, Y. Wang, H. Aleksandrov, J. Szanyi, Clarification of the mechanism of NO reduction with ammonia (SCR) on zeolite catalysts, Chemical Science (2022), https://doi.org/10.1039/D2SC00350C.
[43] B. Ipek, R.F. Lobo, Catalytic conversion of methane to methanol on Cu-SSZ-13 using N_2O as oxidant, Chem. Commun. 52 (2016) 13401–13404, https://doi.org/10.1039/c6cc07893a.
[44] K. Narsimhan, K. Iyoki, K. Dinh, Y. Román-Leshkov, Catalytic oxidation of methane into methanol over copper-exchanged zeolites with oxygen at low temperature, ACS Cent. Sci. 2 (2016) 424–429, https://doi.org/10.1021/acscentsci.6b00139.
[45] K.T. Dinh, M.M. Sullivan, K. Narsimhan, P. Serna, R.J. Meyer, M. Dincă, Y. Román-Leshkov, Continuous partial oxidation of methane to methanol catalyzed by diffusion-paired copper dimers in copper-exchanged zeolites, J. Am. Chem. Soc. 141 (2019) 11641–11650, https://doi.org/10.1021/jacs.9b04906.
[46] A. Koishybay, D.F. Shantz, Water Is the oxygen source for methanol produced in partial oxidation of methane in a flow reactor over Cu-SSZ-13, J. Am. Chem. Soc. 142 (2020) 11962–11966, https://doi.org/10.1021/jacs.0c03283.
[47] R. Oord, J.E. Schmidt, B.M. Weckhuysen, Methane-to-methanol conversion over zeolite Cu-SSZ-13, and its comparison with the selective catalytic reduction of NO_x with NH_3, Catal Sci. Technol. 8 (2018) 1028–1038, https://doi.org/10.1039/C7CY02461D.
[48] S.S. Arora, D.L.S. Nieskens, A. Malek, A. Bhan, Lifetime improvement in methanol-to-olefins catalysis over chabazite materials by high-pressure H_2 co-feeds, Nat. Catal. 1 (2018) 666–672, https://doi.org/10.1038/s41929-018-0125-2.
[49] A.R. Kulkarni, Z.-J. Zhao, S. Siahrostami, J.K. Nørskov, F. Studt, Monocopper active site for partial methane oxidation in Cu-exchanged 8MR zeolites, ACS Catal. 6 (2016) 6531–6536, https://doi.org/10.1021/acscatal.6b01895.
[50] S. Grundner, M.A.C. Markovits, G. Li, M. Tromp, E.A. Pidko, E.J.M. Hensen, A. Jentys, M. Sanchez-Sanchez, J.A. Lercher, Single-site trinuclear copper oxygen clusters in mordenite for selective conversion of methane to methanol, Nat. Commun. 6 (2015) 7546, https://doi.org/10.1038/ncomms8546.
[51] G. Li, P. Vassilev, M. Sanchez-Sanchez, J.A. Lercher, E.J.M. Hensen, E.A. Pidko, Stability and reactivity of copper oxo-clusters in ZSM-5 zeolite for selective methane oxidation to methanol, J. Catal. 338 (2016) 305–312, https://doi.org/10.1016/j.jcat.2016.03.014.

[52] K.D. Vogiatzis, G. Li, E.J.M. Hensen, L. Gagliardi, E.A. Pidko, Electronic structure of the $[Cu_3(\mu\text{-}O)_3]^{2+}$ cluster in mordenite zeolite and its effects on the methane to methanol oxidation, J. Phys. Chem. C. 121 (2017) 22295–22302, https://doi.org/10.1021/acs.jpcc.7b08714.
[53] A.J. Knorpp, A.B. Pinar, M.A. Newton, V.L. Sushkevich, J.A. van Bokhoven, Copper-exchanged omega (MAZ) zeolite: copper-concentration dependent active sites and its unprecedented methane to methanol conversion, ChemCatChem. 10 (2018) 5593–5596, https://doi.org/10.1002/cctc.201801809.
[54] V. Vargheese, J. Murakami, K.K. Bando, I.T. Ghampson, G. Yun, Y. Kobayashi, S. T. Oyama, The direct molecular oxygen partial oxidation of CH_4 to dimethyl ether without methanol formation over a Pt/Y_2O_3 catalyst using an NO/NO_2 oxygen atom shuttle, J. Catal. 389 (2020) 352–365, https://doi.org/10.1016/j.jcat.2020.05.021.
[55] V. Vargheese, Y. Kobayashi, S.T. Oyama, The direct partial oxidation of methane to dimethyl ether over Pt/Y_2O_3 catalysts using an NO/O_2 shuttle, Angew Chemie. 132 (2020) 16787–16793, https://doi.org/10.1002/ange.202006020.
[56] G.I. Panov, G.A. Sheveleva, A.S. Kharitonov, V.N. Romannikov, L.A. Vostrikova, Oxidation of benzene to phenol by nitrous oxide over Fe-ZSM-5 zeolites, Appl. Catal. A Gen. 82 (1) (1992) 31–36, https://doi.org/10.1016/0926-860X(92)80003-U.
[57] Y. Li, W.K. Hall, Catalytic decomposition of nitric oxide over Cu-zeolites, J. Catal. 215 (1991) 202–215, https://doi.org/10.1016/0021-9517(91)90024-X.
[58] B. Wichterlova, J. Dedecek, A. Vondrova, Identification of Cu sites in ZSM-5 active in NO decomposition, J. Phys. Chem. 99 (1995) 1065–1067, https://doi.org/10.1021/j100004a001.
[59] B. Moden, P. Da Costa, B. Fonf, D.K. Lee, E. Iglesia, Kinetics and mechanism of steady-state catalytic NO decomposition reactions on Cu–ZSM5, J. Catal. 209 (2002) 75–86, https://doi.org/10.1006/jcat.2002.3622.
[60] D.K. Lee, Quantification and redox property of the oxygen-bridged Cu^{2+} dimers as the active sites for the NO decomposition over Cu-ZSM-5 catalysts, Korean J. Chem. Eng. 21 (2004) 611–620, https://doi.org/10.1007/BF02705495.
[61] G. Moretti, G. Ferraris, G. Fierro, M. Jacono, S. Morpurgo, M. Faticanti, Dimeric Cu(I) species in Cu-ZSM-5 catalysts: the active sites for the NO decomposition, J. Catal. 232 (2) (2005) 476–487, https://doi.org/10.1016/j.jcat.2005.03.020.
[62] T. Xue, L. Yang, Zeolite-based materials for the catalytic oxidation of VOCs: A mini review, Front. Chem. 9 (2021), https://doi.org/10.3389/fchem.2021.751581 751581.
[63] D.W. Fickel, R.F. Lobo, Copper coordination in Cu-SSZ-13 and Cu-SSZ-16 investigated by variable-temperature XRD, J. Phys. Chem. C. 114 (2010) 1633–1640, https://doi.org/10.1021/jp9105025.
[64] S.I. Zones, Zeolite SSZ-13 and its Method of Preparation, 4,544,538, 1985.
[65] U. Deka, A. Juhin, E. Eilertsen, H. Emerich, M.A. Green, S.T. Korhonen, B.M. Weckhuysen, A.M. Beale, Confirmation of isolated Cu^{2+} Ions in SSZ-13 zeolite as active sites in NH_3-selective catalytic reduction, J. Phys. Chem. C. 116 (2012) 4809–4818, https://doi.org/10.1021/jp212450d.
[66] S.A. Bates, W.N. Delgass, F.H. Ribeiro, J.T. Miller, R. Gounder, Methods for NH_3 titration of Brønsted acid sites in Cu-zeolites that catalyze the selective catalytic reduction of NO_x with NH_3, J. Catal. 312 (2014) 26–36, https://doi.org/10.1016/j.jcat.2013.12.020.
[67] J.R. Di Iorio, S.A. Bates, A.A. Verma, W.N. Delgass, F.H. Ribeiro, J.T. Miller, R. Gounder, The dynamic nature of brønsted acid sites in Cu–zeolites during NO_x selective catalytic reduction: quantification by gas-phase ammonia titration, Top. Catal. 58 (2015) 424–434, https://doi.org/10.1007/s11244-015-0387-8.
[68] L.N. Wilcox, S.H. Krishna, C.B. Jones, R. Gounder, Mechanistic studies of NH_3-assisted reduction of mononuclear Cu(II) cation sites in Cu-CHA zeolites, Catal Sci. Technol. 11 (2021) 7932–7942, https://doi.org/10.1039/d1cy01646f.
[69] T. Beutel, J. Sarkany, G.-D. Lei, J.Y. Yan, W.M.H. Sachtler, J. Sa, Redox chemistry of Cu/ZSM-5, J. Phys. Chem. 100 (1996) 845–851, https://doi.org/10.1021/jp952455u.
[70] P. Da Costa, B. Modén, G.D. Meitzner, D.K. Lee, E. Iglesia, Spectroscopic and chemical characterization of active and inactive Cu species in NO decomposition catalysts based on Cu-ZSM5, Phys. Chem. Chem. Phys. 4 (2002) 4590–4601, https://doi.org/10.1039/b203700a.
[71] J. Wang, V.F. Kispersky, W. Nicholas Delgass, F.H. Ribeiro, Determination of the Au active site and surface active species via operando transmission FTIR and isotopic transient experiments on 2.3 wt.% Au/TiO_2 for the WGS reaction, J. Catal. 289 (2012) 171–178, https://doi.org/10.1016/j.jcat.2012.02.008.
[72] V.J. Cybulskis, J.W. Harris, Y. Zvinevich, A transmission infrared cell design for temperature-controlled adsorption and reactivity studies on heterogeneous catalysts, 103101 (2016). doi:10.1063/1.4963665.
[73] H.A. Massaldi, J.A. Maymo, Error in handling finite conversion reactor data by the differential method, J. Catal. 14 (1969) 61–68, https://doi.org/10.1016/0021-9517(69)90356-X.
[74] F.H. Ribeiro, A.E. Schach von Wittenau, C.H. Bartholomew, G.A. Somorjai, Reproducibility of turnover rates in heterogeneous metal catalysis: compilation of data and guidelines for data analysis, Catal. Rev. 39 (2006) 49–76, https://doi.org/10.1080/01614949708006468.
[75] H.S. Fogler, Essentials of chemical reaction engineering, Pearson Education (2010).
[76] V.J. Cybulskis, A.D. Smeltz, Y. Zvinevich, R. Gounder, W.N. Delgass, F.H. Ribeiro, Learning the fundamentals of kinetics and reaction engineering, Chem. Eng. Eduation. (2016) 202–210.
[77] D.A. Hickman, J.C. Degenstein, F.H. Ribeiro, Fundamental principles of laboratory fixed bed reactor design, Curr. Opin. Chem. Eng. 13 (2016) 1–9, https://doi.org/10.1016/j.coche.2016.07.002.
[78] J.W. Harris, A.A. Verma, J.W. Arvay, A.J. Shih, W.N. Delgass, F.H. Ribeiro, Consequences of product inhibition in the quantification of kinetic parameters, J. Catal. 389 (2020) 468–475, https://doi.org/10.1016/j.jcat.2020.06.014.
[79] N. Akter, X. Chen, J. Parise, J.A. Boscoboinik, T. Kim, Effects of copper loading on NH_3-SCR and NO oxidation over Cu impregnated CHA zeolite, Korean J. Chem. Eng. 34 (2017) 1–10, https://doi.org/10.1007/s11814-017-0268-x.
[80] J.A. Loiland, R.F. Lobo, Low temperature catalytic NO oxidation over microporous materials, J. Catal. 311 (2014) 412–423, https://doi.org/10.1016/j.jcat.2013.12.013.
[81] J.A. Loiland, R.F. Lobo, Oxidation of zeolite acid sites in NO/O_2 mixtures and the catalytic properties of the new site in NO oxidation, J. Catal. 325 (2015) 68–78, https://doi.org/10.1016/j.jcat.2015.02.009.
[82] H. Tsukahara, T. Ishida, M. Mayumi, Gas-phase oxidation of nitric oxide: chemical kinetics and rate constant, Nitric Oxide. 3 (3) (1999) 191–198.
[83] H. Li, C. Paolucci, I. Khurana, L.N. Wilcox, F. Göltl, J.D. Albarracin-Caballero, A.J. Shih, F.H. Ribeiro, R. Gounder, W.F. Schneider, Consequences of exchange-site heterogeneity and dynamics on the UV-visible spectrum of Cu-exchanged SSZ-13, Chem. Sci. 10 (2019) 2373–2384, https://doi.org/10.1039/c8sc05056b.
[84] P.A. Jacobs, H.K. Beyer, Evidence for the nature of true Lewis sites in Faujasite-type zeolites, J. Phys. Chem. 83 (1979) 1174–1177, https://doi.org/10.1021/j100472a013.
[85] J. Sárkány, J.L. d'Itri, W.M.H. Sachtler, Redox chemistry in excessively ion-exchanged Cu/Na-ZSM-5, Catal. Letters. 16 (1992) 241–249, https://doi.org/10.1007/BF00764336.
[86] F. Göltl, S. Bhandari, E.A. Lebrón-Rodríguez, J.I. Gold, S.I. Zones, I. Hermans, J.A. Dumesic, M. Mavrikakis, Identifying hydroxylated copper dimers in SSZ-13 via UV-vis-NIR spectroscopy, Catal. Sci. Technol. 12 (9) (2022) 2744–2748.
[87] M.H. Mahyuddin, G. Saputro, R. Pamungkas, P. Sukanli, F. Fathurrahman, J. Rizkiana, A. Nuruddin, H.K. Dipojono, Molecular insight into the role of zeolite lattice constraints on methane activation over the Cu-O-Cu active site, Phys. Chem. Chem. Phys. 24 (2022) 4196–4203, https://doi.org/10.1039/d1cp05371j.
[88] F. Göltl, S. Bhandari, M. Mavrikakis, Thermodynamics perspective on the stepwise conversion of methane to methanol over Cu-exchanged SSZ-13, ACS Catal. 11 (2021) 7719–7734, https://doi.org/10.1021/acscatal.1c00691.
[89] F. Polo-Garzon, S. Luo, Y. Cheng, K.L. Page, A.J. Ramirez-Cuesta, P.F. Britt, Z. Wu, Neutron scattering investigations of hydride species in heterogeneous catalysis, Neutron Scatt Investig. Hydride Species Heterog. Catal. 12 (2019) 93–103, https://doi.org/10.1002/cssc.201801890.
[90] S.F. Parker, P. Collier, Applications of neutron scattering in catalysis: where atoms are and how they move, Johnson Matthey Technol. Rev. 60 (2016) 132–144, https://doi.org/10.1595/205651316X691230.
[91] P. Sabatier, La catalyse en chimie organique, Berange, Paris. (1920).
[92] R. Villamaina, U. Iacobone, I. Nova, M. Pia Ruggeri, J. Collier, D. Thompsett, E. Tronconi, Low-T CO oxidation over Cu−CHA catalysts in presence of NH_3: probing the mobility of Cu^{II} ions and the role of multinuclear Cu^{II} species, ChemCatChem. 12 (2020) 3843–3848, https://doi.org/10.1002/cctc.202000734.
[93] W. Hu, U. Iacobone, F. Gramigni, Y. Zhang, X. Wang, S. Liu, C. Zheng, I. Nova, X. Gao, E. Tronconi, Unraveling the hydrolysis of Z_2Cu^{2+} to $ZCu^{2+}(OH)^-$ and its consequences for the low-temperature selective catalytic reduction of NO on Cu-CHA catalysts, ACS Catal. 11 (2021) 11616–11625, https://doi.org/10.1021/acscatal.1c02761.
[94] A.J. Shih, Synthesis and Characterization of Copper-Exchanged Zeolite Catalysts and Kinetic Studies on NO_x Selective Catalytic Reduction with Ammonia, Purdue University (2018), https://doi.org/10.25394/PGS.7464596.v1.
[95] J. Luo, F. Gao, K. Kamasamudram, N. Currier, C.H.F. Peden, A. Yezerets, New insights into Cu/SSZ-13 SCR catalyst acidity. Part I: Nature of acidic sites probed by NH_3 titration, J. Catal. 348 (2017) 291–299, https://doi.org/10.1016/j.jcat.2017.02.025.
[96] J. Song, Y. Wang, E.D. Walter, N.M. Washton, D. Mei, L. Kovarik, M.H. Engelhard, S. Prodinger, Y. Wang, C.H.F. Peden, F. Gao, Toward rational design of Cu/SSZ-13 selective catalytic reduction catalysts: implications from atomic-level understanding of hydrothermal stability, ACS Catal. 7 (2017) 8214–8227, https://doi.org/10.1021/acscatal.7b03020.
[97] H. Zhang, J. Lv, Z. Zhang, C. Du, S. Wang, J. Lin, S. Wan, Y. Wang, H. Xiong, Oxidation of Methane to Methanol by Water Over Cu/SSZ-13: Impact of Cu Loading and Formation of Active Sites, ChemCatChem. 14 (2022) e202101609. doi:10.1002/cctc.202101609.
[98] S.C. Larsen, A. Aylor, A.T. Bell, J. a. Reimer, Electron Paramagnetic Resonance Studies of Copper Ion-Exchanged ZSM-5, J. Phys. Chem. 98 (1994) 11533–11540. doi:10.1021/j100095a039.
[99] D.T. Bregante, L.N. Wilcox, C. Liu, C. Paolucci, R. Gounder, D.W. Flaherty, Dioxygen activation kinetics over distinct Cu site types in Cu-chabazite zeolites, ACS Catal. 11 (2021) 11873–11884, https://doi.org/10.1021/acscatal.1c03471.

[100] A.R. Fahami, I. Nova, E. Tronconi, A kinetic modeling study of NO oxidation over a commercial Cu-CHA SCR catalyst for diesel exhaust after treatment, Catal. Today. 297 (2017) 10–16, https://doi.org/10.1016/j.cattod.2017.05.098.
[101] M.P. Ruggeri, I. Nova, E. Tronconi, J.A. Pihl, T.J. Toops, W.P. Partridge, In-situ DRIFTS measurements for the mechanistic study of NO oxidation over a commercial Cu-CHA catalyst, Appl. Catal. B Environ. 166–167 (2015) 181–192, https://doi.org/10.1016/j.apcatb.2014.10.076.
[102] J. Szanyi, J.H. Kwak, H. Zhu, C.H.F. Peden, Characterization of Cu-SSZ-13 NH_3 SCR catalysts: an in situ FTIR study, Phys. Chem. Chem. Phys. 15 (2013) 2368–2380, https://doi.org/10.1039/c2cp43467a.
[103] H. Sjövall, E. Fridell, R.J. Blint, L. Olsson, Identification of adsorbed species on Cu-ZSM-5 under NH_3 SCR conditions, Top. Catal. 42–43 (2007) 113–117, https://doi.org/10.1007/s11244-007-0162-6.
[104] J. Szanyi, M.T. Paffett, The adsorption of NO and reaction of NO with O_2 on H-, NaH-, CuH-, and Cu-ZSM-5: An in situ FTIR investigation, J. Catal. 164 (1996) 232–245, https://doi.org/10.1006/jcat.1996.0378.
[105] K. Hadjiivanov, D. Klissurski, G. Ramis, G. Busca, Fourier transform IR study of NO_x adsorption on a CuZSM-5 $DeNO_x$ catalyst, Appl. Catal. B Environ. 7 (1996) 251–267, https://doi.org/10.1016/0926-3373(95)00034-8.
[106] C. Negri, A. Martini, G. Deplano, K.A. Lomachenko, T.V.W. Janssens, E. Borfecchia, G. Berlier, S. Bordiga, Investigating the role of Cu-oxo species in Cu-nitrate formation over Cu-CHA catalysts, Phys. Chem. Chem. Phys. 23 (2021) 18322–18337, https://doi.org/10.1039/d1cp01754c.